ARTICLE NO. 78-1195R

Spanwise Lift Distribution on a Wing from Flowfield Velocity Surveys

Kenneth L. Orloff*
NASA Ames Research Center, Moffett Field, Calif.

The application of the incompressible three-dimensional momentum integral equation to a finite wing is reviewed. The objective is to interpret the resulting equations in a way that suggests an alternate experimental method for determining the spanwise distribution of lift. Consideration is given to constraints that must be placed on the character of the vortex wake of the wing to provide the familiar relationship between lift and bound vorticity. A novel technique is then presented for obtaining, from behind the wing, the spanwise lift distribution from velocity surveys that are made over only a short distance above and below the wing trailing edge. The necessary formalism is developed to use these measured values to obtain the actual span loading by using an equivalent single-horseshoe vortex model to account for the unmeasured portion of the downward (or upward) momentum. The results of a numerical simulation are presented for a typical loading distribution. The technique is then verified experimentally using laser velocimeter data for the flowfield around a model wing.

Nomenclature

b = wing span
c = local wing chord
$\bar{c}$ = mean geometric chord
c_l = section lift coefficient
C = closed circuit around a wing section
CA = correction accuracy
C_L = total wing lift coefficient
$\mathbf{dl}$ = infinitesimal length vector for line integrations, nondimensionalized by $\bar{c}$
$I(\ )$ = integral operator
L = section lift
L_i = portion of circuit C, where $i=1,2,3,4$
$\hat{n}$ = outward unit normal to surface S
p = static pressure
p_0 = total pressure at infinity
p_T = local total pressure
q_∞ = freestream dynamic pressure
S = control surface
S_i = portion of control surface S, where $i=1,\ldots,6$
S_w = wing surface
$T_\pm$ = correction function
$\mathbf{u}$ = Eulerian fluid velocity
u_x = streamwise component of $\mathbf{u}$, positive downstream
u_y = spanwise component of $\mathbf{u}$, positive outboard
u_z = vertical component of $\mathbf{u}$, positive upward
U_x, U_y, U_z = $\frac{u_x}{V_\infty}, \frac{u_y}{V_\infty}, \frac{u_z}{V_\infty}$,
V = control volume
V_∞ = freestream velocity
x,y,z = Cartesian coordinates
$\hat{x},\hat{y},\hat{z}$ = unit vectors along Cartesian directions x,y,z, respectively
X,Y,Z = $(x/\bar{c}), (y/\bar{c}), (z/\bar{c})$
Y_0 = spanwise location of trailing portion of a horseshoe vortex
γ = nondimensional vortex strength, $cc_l/\bar{c}/8\pi$
Γ = strength of vortex filament; circulation
δ_a, δ_f = deflection angles for ailerons and flaps, positive downward
ζ = nondimensional vorticity vector
$\zeta_x, \zeta_y, \zeta_z$ = Cartesian components of ζ
ρ = fluid density
$\overleftrightarrow{\tau}$ = shear stress tensor

Subscript

e = equivalent vortex

Presented as Paper 78-1195 at the AIAA 11th Fluid and Plasma Dynamics Conference, Seattle, Wash., July 10-12, 1978; submitted Nov. 13, 1979; revision received March 17, 1980. This paper is declared a work of the U.S. Government and therefore is in the public domain.

Index categories: Aerodynamics; Subsonic Flow.

*Research Scientist, Large-Scale Aerodynamics Branch. Member AIAA.

Introduction

THIS paper deals with the application of the momentum integral equation to a wing that is generating lift. The objective is to interpret the resulting lift equation in a way that suggests a reasonable experimental technique for determining the spanwise distribution of lift. The equations for drag and lateral force are not considered in this paper, but are discussed in a separate publication.[1]

Using the concepts of momentum and vorticity to characterize the flow about a wing is by no means new. Lanchester[2] correctly described the mechanism of vortex shedding and rollup in 1909. In 1921, Prandtl[3] implemented enough simplification (lifting-line approximation) successfully to construct an analytical method that relates this shedding process to the spanwise loading distribution. However, some investigators such as Munk[4] in 1924, felt that the bound vortex concept was only a convenient means for qualitatively describing the flow, and that there was "no longer any reason for the use of vortices in the computations in connection with airplane wings." In spite of this, in 1925 Bryant and Williams[5] successfully obtained the lift on an airfoil by measuring along a contour enclosing the airfoil. To this author's knowledge, since these early efforts, very little progress has been made to experimentally implement these ideas.

This paper extends these early ideas to eliminate the closed contour. The loading distribution on a wing is shown to be obtainable from flow surveys made behind the wing only; these results are then augmented with the help of a high-speed computer to complete the contour analytically.

The motivation for reconsidering these early concepts has been due largely to the success of the laser velocimeter in conducting wind-tunnel flow diagnostics. Probe-type measuring devices are cumbersome to use for making closed circulation paths. Additionally, these devices often lack the

required sensitivity and accuracy. The advent of the laser velocimeter, however, provides a more practical and accurate means for remotely conducting the required flow measurements.

It is hoped that this paper will demonstrate that the ideas of Lanchester and Prandtl are still viable. Perhaps it has only been the drawbacks of conventional anemometers that have hindered further exploitation of these fundamental relationships.

Momentum Analysis

In the absence of any net body force, the integral form of the steady momentum equation may be written as

$$\oint_S \rho u(u\cdot\hat{n})\,dS = -\oint_S p\hat{n}\,dS + \oint_S (\hat{n}\cdot\vec{\tau})\,dS \qquad (1)$$

where $\vec{\tau}$ is the shear stress tensor at points on a closed surface S surrounding a volume V; $\hat{n}$ is the outward unit normal to the surface S; p is the static pressure; ρ the fluid density, and u the Eulerian fluid velocity.

Figure 1 depicts the control surface to be used for computing the sectional lift. The influences of the wing on the fluid are represented by corresponding variations in the velocities, static pressures, and shearing stresses on the control surface. Whereas the wing surface S_w forms a part of the closed surface S, the portions on S_5 and S_6 that include the airfoil cross section are *not* part of the closed control surface.

Reference 1 verifies that the last term in Eq. (1) is negligible on surfaces S_1 through S_6 when the flow Reynolds number (based on mean chord) is large. Also, we assume any lift generated over the wing surface S_w by shearing forces to be negligible compared to the pressure lift. Then, the z component of Eq. (1) becomes

$$L = \int_{S_1} \rho u_x u_z\,dy\,dz - \int_{S_2} (\rho u_z^2 + p)\,dx\,dy - \int_{S_3} \rho u_x u_z\,dy\,dz + \int_{S_4} (\rho u_z^2 + p)\,dx\,dy + \int_{S_5} \rho u_y u_z\,dx\,dz - \int_{S_6} \rho u_y u_z\,dx\,dz \qquad (2)$$

where we have equated the static pressure integration over S_w to minus the section lift L.

For the control surface of Fig. 1, the differential dy becomes Δy and the area integrations over S_1, S_2, S_3, and S_4 become line integrations along L_1, L_2, L_3, and L_4, respectively, with width Δy. Hence, L can be written as $L = q_\infty c_l c \Delta y$, where c_l is the section lift coefficient and c the local chord. Furthermore, the second and fourth terms in Eq. (2) require a knowledge of the static pressure on the control surface. Experimentally, these pressures would be difficult to measure accurately; undetected, small changes over a large surface area can produce a considerable error in the resulting force computation. Since the accurate measurement of the velocity is more convenient (especially with the laser velocimeter), the static pressures in Eq. (2) are replaced with the total pressure and the local velocity

$$p = p_T - \frac{\rho}{2}(u_x^2 + u_y^2 + u_z^2)$$

This substitution is helpful in two ways: 1) a difficult measurement has been replaced by simpler ones; 2) the total pressure p_T is the total head p_0 in all regions that have not suffered viscous losses. Using these substitutions for lift and static pressure, respectively, and nondimensionalizing all velocities by V_∞ and x, y, and z by $\bar{c}$, the mean geometric chord, Eq. (2) reduces to

$$\frac{cc_l}{\bar{c}} = 2\int_{L_1} U_x U_z\,dZ - \int_{L_2} (U_z^2 - U_x^2 - U_y^2)\,dX - 2\int_{L_3} U_x U_z\,dZ + \int_{L_4} (U_z^2 - U_x^2 - U_y^2)\,dX + \frac{2}{\Delta Y}\left[\int_{S_5} U_y U_z\,dX\,dZ - \int_{S_6} U_y U_z\,dX\,dZ\right] \qquad (3)$$

The total pressure does not appear in Eq. (3) because it has the same value p_0 on both S_2 and S_4.

The assumption is now made that the flow velocity around the wing changes smoothly and slowly enough with respect to Y that the integrands in the surface integrals of Eq. (3) can be expressed, to the first order, as

$$(U_y U_z)_6 = (U_y U_z)_5 + \left[\frac{\partial}{\partial Y}(U_y U_z)\right]_S \Delta Y \qquad (4)$$

where subscripts 5 and 6 refer to surfaces S_5 and S_6, respectively, and subscript S indicates evaluation of the derivative at the surface spanned by the closed circuit C defined by L_1, L_2, L_3, and L_4. The normal to S is taken in the positive y direction. Substituting Eq. (4) into the surface integration of Eq. (3),

$$\frac{2}{\Delta Y}\left(\int_{S_5} U_y U_z\,dX\,dZ - \int_{S_6} U_y U_z\,dX\,dZ\right) = -2\int_S \frac{\partial}{\partial Y}(U_y U_z)\,dX\,dZ \qquad (5)$$

Reference 1 develops an alternate expression for the surface integral on the right-hand side of Eq. (5) that reduces Eq. (3)

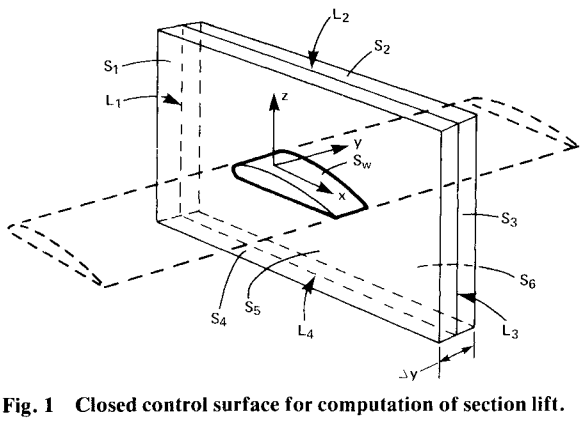

Fig. 1 Closed control surface for computation of section lift.

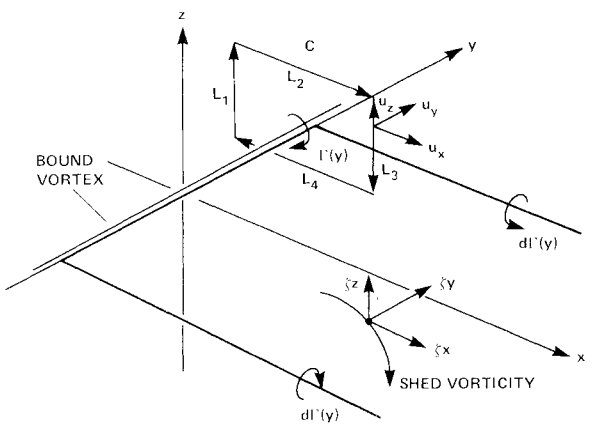

Fig. 2 Lifting-line approximation showing integration circuit C, bound and shed vorticity.

to

$$\frac{cc_l}{\bar{c}} = 2\int\int_S (U_x\zeta_y - U_y\zeta_x)\,dX\,dZ \tag{6}$$

where $\zeta = \text{curl } U$ is the nondimensional vorticity vector.

Equation (6) is not in a form that suggests a reasonable experimental technique for determining the section lift coefficient c_l. The method implied by this expression would require detailed distributions of the velocity field over the entire surface S. The need for the vorticity distributions would require that the derivatives of the velocity be determined from the data, reducing the accuracy of the results. Hence, before our analysis can continue, some assumptions must be made regarding the character of the flow in order to further simplify Eq. (6).

Lifting-Line Approximation

If the flowfield of interest can be adequately described by a lifting-line model (at least over the region enclosed by the closed circuit C), then Eq. (6) can be simplified considerably. The assumed geometry, shown in Fig. 2, reduces the wing cross-sectional area to zero about the bound vortex. The surface denoted by the double integration in Eq. (6) is therefore the entire area spanned by C. This allows the use of Stokes's theorem, which reduces the problem to a line integral around C, if Eq. (6) can be put into a form that is compatible with this theorem.

To apply Stokes's theorem, two implicit restrictions of the lifting-line model are noted:

1) If the lines of shed vorticity are allowed downward deflection due to mutual induction, but spanwise deflection is forbidden, then ζ_y is nonzero only along the bound vortex. Hence, it is only nonzero at $X=Z=0$, where $U_x=1$.

2) ζ_x vanishes along the bound vortex. It is nonzero only along a trailing line of shed vorticity of strength $d\Gamma(y)$. However, if no spanwise wake deflection is allowed, then $U_y=0$ along these lines. Using these two restrictions, the lift coefficient is

$$\frac{cc_l}{\bar{c}} = 2\int\int_S (U_x\zeta_y - U_y\zeta_x)\,dX\,dZ = 2\int\int_S \zeta_y\,dX\,dZ$$

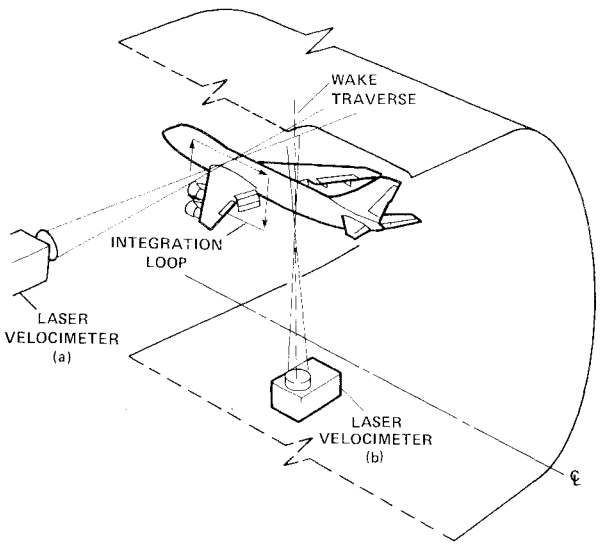

Fig. 3 Experimental situation that allows for either spanwise or limited optical access: a) spanwise optical access (typical of smaller facilities, e.g., Ames 7×10 ft wind tunnel): section lift coefficient can be determined from $(cc_l)/\bar{c} = 2\oint_C U\cdot dl$; b) limited optical access (typical of larger facilities, e.g., Ames 40×80 ft wind tunnel): section lift coefficient determined by correcting measured $(cc_l)\bar{c}$ using an equivalent vortex.

Writing $\zeta_y = \hat{y}\cdot\text{curl } U$, Stokes's theorem may be applied,

$$\frac{cc_l}{\bar{c}} = 2\int\int_S \hat{y}\cdot\text{curl}\,U\,dX\,dZ = 2\oint_C U\cdot dl \tag{7}$$

where $\hat{y}$ is precisely the unit normal to the surface S. This is a familiar result for two-dimensional flows, but it is also valid for a three-dimensional flow with the two lifting-line restrictions above.

At this juncture in the analysis, the lifting-line model and Eq. (7) do not account for the presence of the vorticity contained in the free viscous wake. In 1925, Taylor[6] showed that an additional constraint must be placed on the type of contour C chosen if the effects of the wake are not to introduce error into the lift coefficient obtained using Eq. (7); that is, the contour must be chosen so that the part that cuts the wake is a straight line perpendicular to the relative wind. Equivalently, the wake must be crossed such that equal amounts of positive and negative vorticity are carried across the boundary and away from the neighborhood of the airfoil by the fluid in the wake. In the present analysis, L_3 meets the necessary criteria.

If the lifting-line model is assumed to represent the real flow adequately, at least in the region of the control surface, then Eq. (7) suggests that the section lift coefficient can be determined experimentally by measuring the appropriate velocity components on the closed contour C. If the orientation of the loop remains rectilinear to the flow, then the extent of circuit C is not restricted as long as the vorticity passing through it remains constant. As the loop expands, however, the velocity variation about freestream conditions becomes smaller; to sense these changes with sufficient accuracy to perform the integration in Eq. (7) becomes increasingly difficult.

To measure the flow velocities along the loop C with a laser velocimeter, spanwise optical access to the flow must be possible, as indicated in Fig. 3. Such a view of the selected spanwise location may, however, be hindered by obstacles such as engine nacelles and flaps. To measure around these obstacles, the loop may become so large that the accuracy of the measurement is compromised. Additionally, spanwise access may not be feasible, as in a large wind tunnel (e.g., Ames 40×80 ft wind tunnel). Hence, it is convenient to extend the results of the previous sections to the spanwise loading when only limited optical access is available. This extension is accomplished in the following section.

Computation of the "Unmeasured" Momentum

Equation (7) may be written as

$$\frac{cc_l}{\bar{c}} = 2\oint_C U\cdot dl$$

$$= 2\left(\int_{L_1} U_z\,dZ + \int_{L_2} U_x\,dX - \int_{L_3} U_z\,dZ - \int_{L_4} U_x\,dX\right)$$

If the boundaries L_1,L_2, and L_4 are far removed from the vicinity of the wing, then $U_z=0$ on L_1 and $U_x=1$ on L_2 and L_4. Hence,

$$\frac{cc_l}{\bar{c}} = -2\int_{L_3} U_z\,dZ = -2\int_{-\infty}^{\infty} U_z\,dZ \tag{8}$$

Because an experimental traverse along L_3 can be made over only a finite distance between Z_1 and Z_2 (see Fig. 4), Eq. (8) is written as

$$\frac{cc_l}{\bar{c}} = -2\int_{Z_2}^{\infty} U_z\,dZ - 2\int_{-\infty}^{Z_1} U_z\,dZ + \left(\frac{cc_l}{\bar{c}}\right)_{\text{meas}} \tag{9}$$

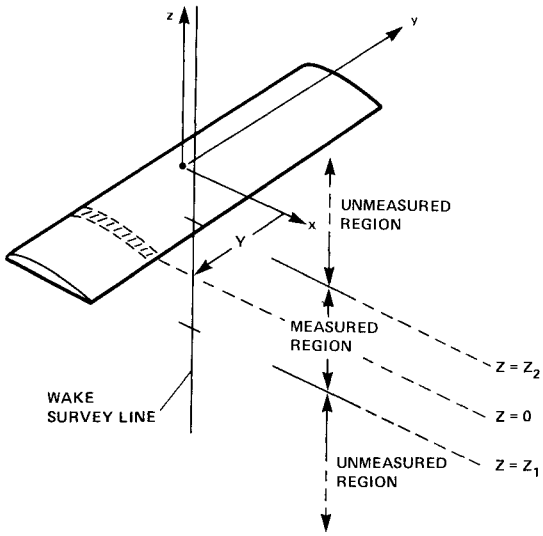

Fig. 4 Measured region determined by finite length of experimental traverse over portion of wake survey line. Flow is modeled in unmeasured regions to generate numerical contribution to value of $(cc_l)/\bar{c}$.

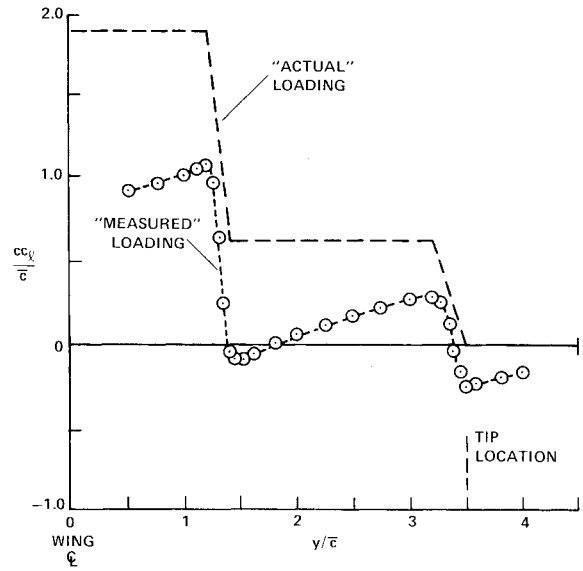

Fig. 5 Difference between "actual" and "measured" loading distribution for finite traverse distance: $Z_2 = -Z_1 = 1.0$; $X = 0.9$.

where

$$\left(\frac{cc_l}{\bar{c}}\right)_{\text{meas}} = -2\int_{Z_1}^{Z_2} U_z \mathrm{d}Z$$

is the "measured" value between the limits Z_1 and Z_2.† The first and second terms in Eq. (9) relate to the z component of the linear momentum present outside the measured region. This momentum must be accounted for if an accurate value for the section lift coefficient is to be obtained.

The difference to be expected between the true value of $(cc_l)/\bar{c}$ and the measured value

$$(cc_l/\bar{c})_{\text{meas}}$$

can be shown by formulating a computer code to generate a flowfield and then performing the experiment numerically. Reference 1 contains the details of this flowfield generation routine and the relevant equations. This generator allows for a nonplanar wake, but does not allow spanwise vorticity ζ_y in the free wake. The numerical simulation uses this velocity field as a basis for the "measurements." Figure 5 compares a known (actual) $(cc_l)/\bar{c}$ distribution with that determined by a wake survey over a finite distance Z_1 to Z_2. The points for the "measured" loading have been obtained from the simulation routine. The survey limits have been chosen as one mean geometric chord both above and below the "trailing edge"; the survey is made at 0.9 $\bar{c}$ behind the bound vortex. The comparison is understandably poor because a significant portion of downward momentum is contained in the unmeasured region and has been neglected. Also, note that the "measured" loading in Fig. 5 does not extend inboard from $Y = 0.5$. This is intentional since it is unlikely in a real experiment that one could obtain data any closer because of fuselage interference.

Determining the Equivalent Vortex

The difference between the "actual" and "measured" loadings in Fig. 5 can be accounted for by modeling the flow analytically in the unmeasured regions. The parameters of the model are determined by the character of the data obtained in the measured region. The terms in Eq. (9) that represent the numerical contribution can then be computed and the complete lift coefficient determined.

The assumption is made that there exists a single equivalent horseshoe vortex that contains an amount of downward momentum in the unmeasured regions that is very nearly equal to the momentum generated in these regions by the span loading of interest. If it is further assumed that this horseshoe is planar, then the induced velocity component U_z at any point (X, Y, Z) in the flow due to the equivalent system can be shown to be

$$U_{z_e} = -\gamma_e [AX + B(Y_{0_e} - Y) + C(Y_{0_e} + Y)] \qquad (10)$$

where the subscript e refers to the equivalent vortex,

$$\gamma_e = \frac{(cc_l/\bar{c})_e}{8\pi}$$

is the strength of the vortex, Y_{0_e} is the spanwise location of the trailing portion of the horseshoe, and A, B, and C are given by

$$A = \left[\frac{Y_+}{\sqrt{X^2 + Y_+^2 + Z^2}} + \frac{Y_-}{\sqrt{X^2 + Y_-^2 + Z^2}}\right](X^2 + Z^2)^{-1}$$

$$B = \left[\frac{X}{\sqrt{X^2 + Y_-^2 + Z^2}} + 1\right](Y_-^2 + Z^2)^{-1}$$

$$C = \left[\frac{X}{\sqrt{X^2 + Y_+^2 + Z^2}} + 1\right](Y_+^2 + Z^2)^{-1}$$

where $Y_+ = Y_{0_e} + Y$ and $Y_- = Y_{0_e} - Y$.

Substituting Eq. (10) into Eq. (9), gives

$$\frac{cc_l}{\bar{c}} = 2\gamma_e [XI(A) + Y_- I(B) + Y_+ I(C)] + \left(\frac{cc_l}{\bar{c}}\right)_{\text{meas}} \qquad (11)$$

where $I(F)$ is the definite integral operator

$$I(F) = \int_{Z_2}^{\infty} F\mathrm{d}Z + \int_{-\infty}^{Z_1} F\mathrm{d}Z \qquad (12)$$

†Because the experiment is first numerically simulated, the computation of the lift coefficient is referred to as the "measured" value; the quotation marks are intended to distinguish this from an actual wind-tunnel measurement.

The indefinite form of the integrals in Eq. (12) may be evaluated and shown to be

$$\int A\,dZ = \frac{1}{X}\left[\tan^{-1}\left(\frac{Y_+ \sin\theta}{X}\right) + \tan^{-1}\left(\frac{Y_- \sin\phi}{X}\right)\right]$$

$$\int B\,dZ = \frac{1}{Y_-}\left[\tan^{-1}\left(\frac{X\sin\phi}{Y_-}\right) + \tan^{-1}\left(\frac{Z}{Y_-}\right)\right]$$

$$\int C\,dZ = \frac{1}{Y_+}\left[\tan^{-1}\left(\frac{X\sin\theta}{Y_+}\right) + \tan^{-1}\left(\frac{Z}{Y_+}\right)\right] \qquad (13)$$

where

$$\sin\theta = Z/\sqrt{X^2 + Y_+^2 + Z^2}$$

and

$$\sin\phi = Z/\sqrt{X^2 + Y_-^2 + Z^2}$$

With attention being given to the signs of the numerators and denominators in Eq. (13), Eq. (11) can be expressed as

$$\frac{cc_l}{\bar{c}} = -\frac{1}{2\pi}\left(\frac{cc_l}{\bar{c}}\right)_e T_+ + \left(\frac{cc_l}{\bar{c}}\right)_{\text{meas}} \quad \text{for} \quad -Y_{0_e} \le Y \le Y_{0_e}$$

$$\frac{cc_l}{\bar{c}} = -\frac{1}{2\pi}\left(\frac{cc_l}{\bar{c}}\right)_e T_- + \left(\frac{cc_l}{\bar{c}}\right)_{\text{meas}} \quad \text{for} \quad Y > Y_{0_e}$$

$$\frac{cc_l}{\bar{c}} = \frac{1}{2\pi}\left(\frac{cc_l}{\bar{c}}\right)_e T_- + \left(\frac{cc_l}{\bar{c}}\right)_{\text{meas}} \quad \text{for} \quad Y < -Y_{0_e} \qquad (14)$$

where

$$T_\pm = \tan^{-1}\left(\left|\frac{Y_+ \sin\theta_2}{X}\right|\right) + \tan^{-1}\left(\left|\frac{X\sin\theta_2}{Y_+}\right|\right)$$

$$\pm\tan^{-1}\left(\left|\frac{Y_- \sin\phi_2}{X}\right|\right) \pm \tan^{-1}\left(\left|\frac{X\sin\phi_2}{Y_-}\right|\right)$$

$$+\tan^{-1}\left(\left|\frac{Z_2}{Y_+}\right|\right) \pm \tan^{-1}\left(\left|\frac{Z_2}{Y_-}\right|\right) - \pi \mp \pi \qquad (15)$$

This solution is restricted to $Z_2 = -Z_1$; subscript 2 in Eq. (15) denotes evaluation of $\sin\theta$ and $\sin\phi$ at $Z = Z_2$. The distance behind the bound vortex at which the survey has been made is given by X, and Y is the spanwise location where the numerical contribution is desired.

Note from Eqs. (14) and (15) that the numerical contribution is completely determined by specifying two values: $(cc_l/\bar{c})_e$ and Y_{0_e}, the strength and location, respectively, of the equivalent vortex. To obtain these values, two known conditions are invoked relevant to the corrected distribution $(cc_l)/\bar{c}$. These two conditions are:

1) The value of $(cc_l)/\bar{c}$ at the wing tip must be zero.

2) The area beneath the $(cc_l)/\bar{c}$ distribution must be related to the total lift coefficient of the wing C_L according to

$$C_L = \frac{2\bar{c}}{b}\int_0^{b/2\bar{c}} \left(\frac{cc_l}{\bar{c}}\right) dY \qquad (16)$$

The first condition is satisfied only if Y_{0_e} is located inboard of the wing tip. It then follows from the second part of Eq. (14) that

$$\left(\frac{cc_l}{\bar{c}}\right)_e = \frac{2\pi}{T_-}\left(\frac{cc_l}{\bar{c}}\right)_{\text{meas at tip}} \qquad (17)$$

T_- contains both Y_{0_e} and $(cc_l/\bar{c})_e$ so that closure of the solution requires the second condition to be invoked. This is accomplished numerically by iterating the solution, as indicated in Fig. 6.

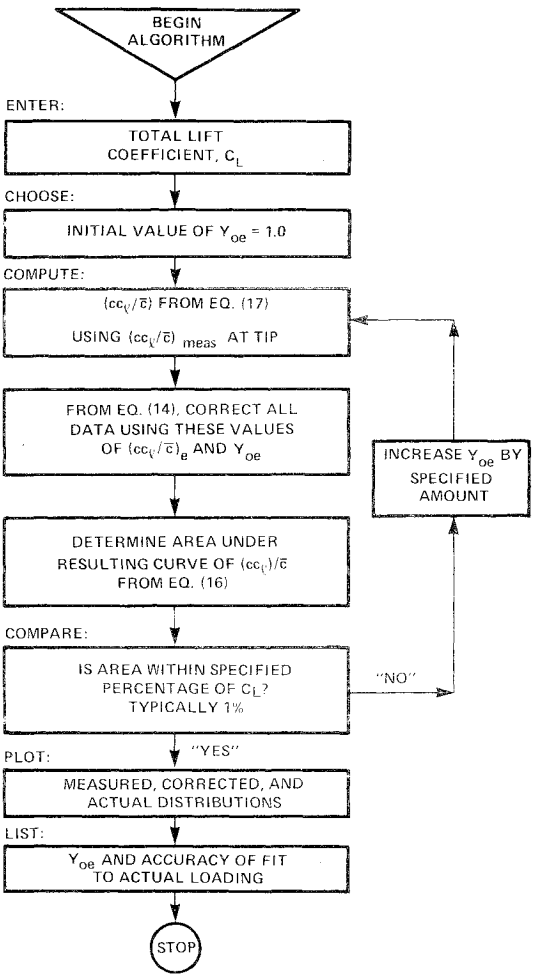

Fig. 6 Algorithm to determine numerical contribution to lift coefficient.

Results from Numerical Experiments

Figure 7 shows the results obtained by applying this iteration scheme to the data in Fig. 5. The equivalent vortex is located at $Y_{0_e} = 2.79$, with a strength $(cc_l/\bar{c})_e = 1.42$. The area beneath the corrected data matches $C_L = 1.08$ to within 1%.

The agreement between the corrected data and the "actual" loading in Fig. 7 is good, except in the areas noted. If, however, the extent of the measured region were greater than $Z_2 = 1.0$, then the correction scheme should be more accurate. To verify this refer to Fig. 8, which shows uncorrected loadings for several survey distances Z_2 from 0.5 to 2.0 chords above and below the wing. Clearly, as survey distance Z_2 increases, more momentum contributes to the "measured" value. Figure 9 presents the corrected loadings for the most extreme values of Z_2 in Fig. 8. As expected, the loading is more faithfully reproduced at $Z_2 = 2.0$ than at $Z_2 = 0.5$.

To quantify the accuracy with which this algorithm reproduces the "actual" loading, the area mismatch in Fig. 7 is used and the following definition is applied:

$$\text{Correction accuracy} = \left(1 - \frac{\text{area mismatch}}{C_L}\right) \times 100\%$$

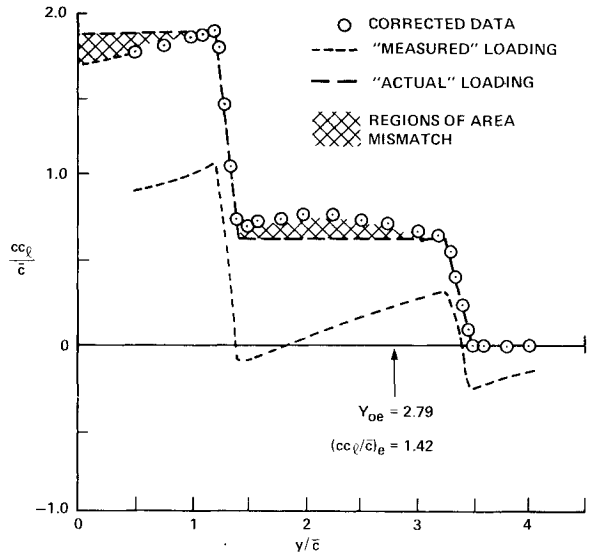

Fig. 7 Corrected data showing comparison to "actual" loading when lift coefficient $C_L = 1.08$ is matched to within 1%.

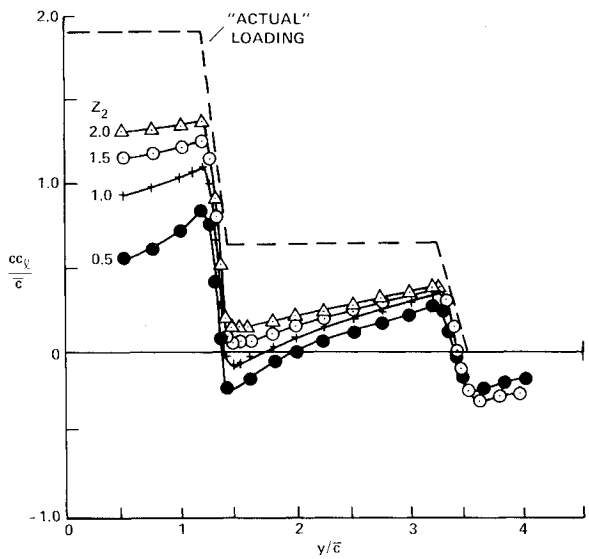

Fig. 8 Uncorrected loading for several survey distances.

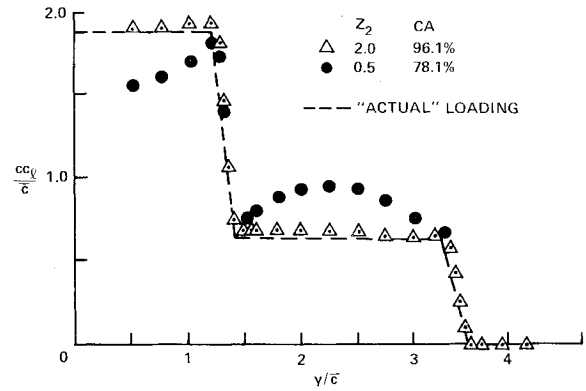

Fig. 9 Corrected loadings showing the increased accuracy of the correction algorithm with increasing survey distance.

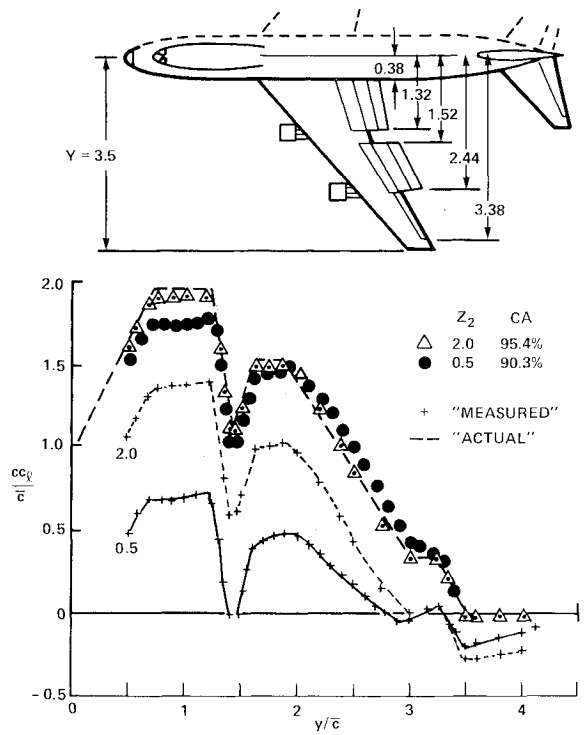

Fig. 10 Equivalent vortex method applied to a typical complex loading distribution (drawing shows assumed locations of shed vortices for flowfield generator; $X = 0.9$).

The correction accuracy (CA) in Fig. 9 indicates a mismatch of less than 4% for the survey of 2.0 chords, compared to more than 20% mismatch for a survey of 0.5 chords.

It is of interest to consider the application of this equivalent vortex technique to a realistic loading distribution, one that more closely approximates a typical aircraft configuration. Numerical wake survey results for this type of loading are presented in Fig. 10. Additional results for several other loadings are presented by Orloff[1] and are summarized in Fig. 11, showing the correction accuracy as a function of survey distance Z_2. These data suggest that as the loading distribution deviates further from the elliptic, the required survey distance must increase to maintain a given percentage accuracy in the agreement with the "actual" distribution. Equivalently, this means that the single vortex equivalent model becomes less adequate as the loading shifts inboard (exhibiting less resemblance to an elliptic loading). On the other hand, an acceptable reproduction of the loading is obtained with the single vortex model when the correction accuracy is greater than about 93%. Therefore, if one were to conduct a wind-tunnel experiment with a laser velocimeter, a minimum survey distance would be required to obtain an accurate (93%) loading distribution. Figure 11 suggests the following guidelines for any loading similar to those presented in Table 1.

Experimental Verification

Apparatus and Procedure

An unswept, tapered, untwisted wing of aspect ratio 6.21 and span of 1.71 m was installed in a 2.13 × 3.05 m (7 × 10 ft) subsonic wind tunnel. The wing taper is 0.5 and the airfoil section is 64_1-212 with forward contour modification.[7] The ailerons are continuously adjustable and the flaps can be set to 0,15,20, or 30 deg. A length of basic section (0.65 $\bar{c}$; $\bar{c} = 27.46$ cm) separates the flap and aileron. In the center of this length, the wing has surface pressure orifices for determining the section lift.

The velocity flowfield around this wing was surveyed with a laser velocimeter that could sense both the streamwise (X) and normal (Z) components of the velocity.[8] The spatial resolution of this instrument is equal to the focal volume dimensions: 0.3 mm diam × 2 mm length (lateral direction).

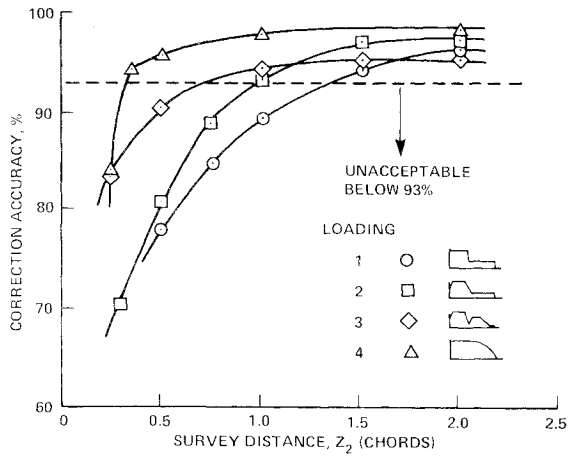

Fig. 11 Accuracy of the equivalent vortex model as a function of survey distance for several loadings.

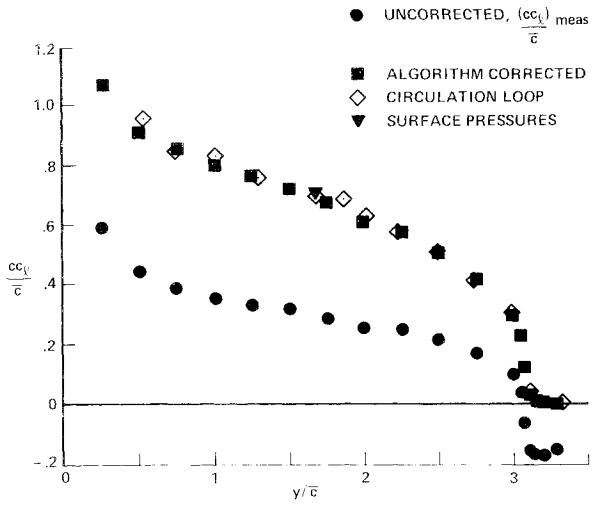

Fig. 12 Experimental results—loading A: $\delta_a = \delta_f = 0$ deg, $\alpha = 6$ deg, $C_L = 0.69$. Traverse distance for wake surveys is $Z_2 = -Z_1 = 1.0$.

Table 1 Minimum survey distance Z_2 above and below wing trailing edge to obtain a specified accuracy for span loading distributions shown in Fig. 11

Loading	Minimum survey distance (chords), 93% accuracy
1	1.4
2	1.0
3	0.8
4	0.3

Table 2 Aileron and flap deflections for three span loading distributions used for experimental verification of equivalent vortex correction algorithm

Loading	δ_a, deg	δ_f, deg
A	0	0
B	0	30
C	20	20

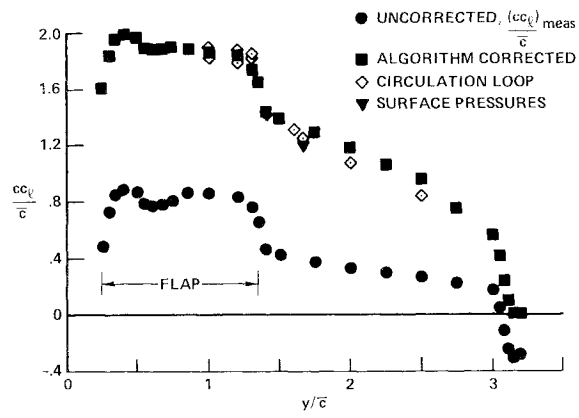

Fig. 13 Experimental results—loading B: $\delta_a = 0$ deg, $\delta_f = 30$ deg, $\alpha = 10$ deg, $C_L = 1.34$. Traverse distance for wake surveys is $Z_2 = -Z_1 = 0.7$.

This focus can be translated laterally with an analog optical scanning controller; motion in the X-Z plane is provided by translation platform with stepping motor control. This latter motion uses a digital interface to a minicomputer with a positioning accuracy of ± 0.05 mm. The velocity data are also acquired through a digital interface, from counter-type laser velocimeter signal processors.

The survey path to be made by the laser velocimeter focal volume is specified before a data sequence; the minicomputer then controls position incrementing and data acquisition along this path. The results are reduced and displayed in real time on a CRT graphics terminal.

This optical arrangement provides spanwise optical access, but the wake survey method can also be tested since the wing trailing edge sweeps forward and the outgoing laser beams are not interrupted when the focus is close behind the wing. A section lift coefficient can be obtained directly by specifying a rectangular survey path ("circulation" loop) of desired dimensions enclosing the airfoil. When the spanwise location of this closed circuit is chosen to be that of the pressure orifices, the accuracy of the result may be assessed by comparison with that determined from an integration of surface pressures. Secondly, the measured section lift coefficient $(cc_l/\bar{c})_{meas}$ can be computed from data along a selected wake survey line with $Z_2 = -Z_1$ at the desired X and Y locations.

Verification of the theory is based on three different loadings that have been studied experimentally. These loadings are denoted and described in Table 2. Loading A was surveyed extensively using circulation loops; loadings B and C were studied in this manner only through regions of high loading gradients. Wake survey traverses were conducted in a detailed fashion over the entire semispan for each loading.

Results

Figure 12 presents the results for loading A. Loading 4 (from Fig. 11) is very similar to loading A, and the numerical analysis suggests that a wake survey distance of only 0.3 $\bar{c}$ is needed to obtain 93% correction accuracy. Experimentally, however, to obtain a more accurate loading, $Z_2 = 1.0$ was used for an anticipated correction accuracy near 98%. Also, as indicated in Fig. 12, many circulation loops were conducted over the semispan to obtain a more precise comparison with the wake survey results. The section loading from surface pressures clearly substantiates the accuracy of the circulation loop method; likewise, the circulation loop data indicate that the wake survey method produces the same loading distribution, thereby validating the algorithm of Fig. 6. Indeed, the expected high degree of accuracy has been achieved using the equivalent vortex method. The convergence time for the algorithm was, in this case, less than 1 min.

Figure 13 shows the results when the flaps are deflected by 30 deg (loading B). Several circulation loops were conducted in the region around the outboard edge of the flap. The loop values inboard of this edge indicate the repeatability in regions of high loading gradients to be better than 5%. Again,

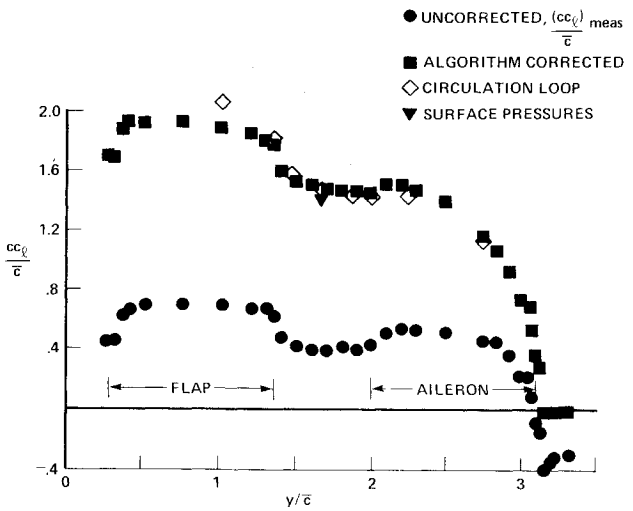

Fig. 14 Experimental results—loading C: $\delta_a = 20$ deg, $\delta_f = 20$ deg, $\alpha = 12$ deg, $C_L = 1.28$. Traverse distance for wake surveys is $Z_2 = -Z_1 = 0.6$.

the surface pressures verify the accuracy of the circulation loop results, and the corrected wake survey data yield a spanwise loading that appears to be within the correction accuracy predicted from Fig. 11 (loading 2, $CA \simeq 88\%$ for $Z_2 = 0.7$). Moreover, the overcorrection produced by the algorithm outboard of this flap edge is similarly predicted by the numerical simulation (see Fig. 9). The decreased loading near $Y = 0.6$ was also observed from tuft studies that revealed a mildly separated flow over the flap at this location with attached flow over the remainder of the flap.

Loading C is characterized by a flap deflection of 20 deg; the ailerons are also deflected downward 20 deg (rather than the opposite deflection). Figure 14 shows that the surface pressure result is again in excellent agreement with the circulation loop value, and that the corrected wake surveys yield an accurate loading distribution. Furthermore, the underestimation of the loading over the flap and the slight overestimation along the aileron are both to be expected for a survey distance of $0.6\,\bar{c}$ (see Fig. 10).

Summary and Limitations

An analysis of the momentum integral equation has shown that the local section lift coefficient on a wing is determined solely by the net vorticity passing through a closed circuit C when certain restrictions are placed on the character of the inviscid wake structure and on the manner in which the viscous wake is traversed. It has been shown that, when downward deflection of the shed vorticity is present, but spanwise deflection is absent within the loop C, the relationship in Eq. (7) is valid. The analysis assumes the bound vortex line to lie along the y axis with $\zeta_x = 0$. The analysis does, however, proceed identically from Eq. (6) when wing sweep is included. In this case, ζ_x has a finite value along the bound vortex, but spanwise deflection of the trailing vortex system is again forbidden, and symmetry provides $U_y = 0$ at all points of the bound vortex. Hence, the example presented for the swept-wing transport-type loading is still meaningful.

These considerations led to the development of a method for determining the spanwise lift distribution from measurements of wake velocities only. The single-horseshoe equivalent vortex method has been shown adequate as long as the wake survey line sufficiently extends far above and below the wing trailing edge. The required survey distance was found to increase as the loading is concentrated further inboard. The algorithm for the correction scheme has been tested using laser velocimeter data for the flow around a model wing; experimentally, the algorithm has been shown to provide an accurate loading distribution for complex as well as simple loadings.

An important advantage of the wake survey technique is the ability to obtain a detailed loading within a transition region between a flapped section and the basic section where the loading gradient is substantial. Examples of such measurements have been presented. To obtain these results using surface pressures would be difficult, especially for small-scale models.

The analysis presented herein assumes a steady fluid flow over the wing. At high angles of attack, however, when unsteady separation is likely to occur (e.g., leading-edge stall), the analysis is no longer applicable. If, however, the separation should occur over only a small region in the neighborhood of the trailing edge, then the circulation within loop C is still related to the section lift as long as the enlarged viscous wake contains equal positive and negative vorticity and the flow remains steady. This condition was encountered with loading B; the loading was determined over the portion of the flapped section experiencing steady trailing-edge stall.

References

[1] Orloff, K.L., "Determining the Lift and Drag Distributions on a Three-Dimensional Airfoil from Flow-Field Velocity Surveys," NASA TM-73,247, May 1977.

[2] Lanchester, F.W., *Aerodynamics,* 2nd ed., Constable & Company, Ltd., London, 1909, p. 178.

[3] Prandtl, L., "Applications of Modern Hydrodynamics to Aeronautics," NACA TR 116, 1921.

[4] Munk, M.M., "Note on Vortices and on Their Relation to the Lift of Airfoils," NACA TN 184, March 1924.

[5] Bryant, L.W. and Williams, D.H., "An Investigation of the Flow of Air Around an Aerofoil of Infinite Span," *Philosophical Transactions of the Royal Society,* A., Vol. CCXXV, 1925, pp. 199-237.

[6] Taylor, G.I., "Note on the Connection Between the Lift on an Aerofoil in a Wind Tunnel and the Circulation Round It," *Philosophical Transactions of the Royal Society,* A, Vol. CCXXV, 1925, pp. 238-245.

[7] Hicks, R.M., Mendoza, J.P., and Bandettini, A., "Effects of Forward Contour Modification on the Aerodynamic Characteristics of the NACA 64_1-212 Airfoil Section," NASA TM X-3293, Sept. 1975.

[8] Grant, G.R. and Orloff, K.L., "Two-Color Dual-Beam Backscatter Laser Doppler Velocimeter," *Applied Optics,* Vol. 12, Dec. 1973, pp. 2913-2916.